Intrinsically disordered regions in the transcription factor MYC:MAX provide DNA selectivity via intramolecular interactions

Stefan Schütz[1,*], Christian Bergsdorf[1], Sandra Hänni-Holzinger[1], Andreas Lingel[1], Martin Renatus[1,2], Alvar D. Gossert[3], Wolfgang Jahnke[1,*]

[1] Novartis Institutes for BioMedical Research, Novartis Campus , CH-4056 Basel, Switzerland.
[2] current adress: Ridgeline Discovery, CH-4057 Basel, Switzerland
[3] ETH Zürich, CH-8093 Zurich, Switzerland

***Corresponding Authors**: Stefan Schütz and Wolfgang Jahnke.
Email: stefan.schuetz@novartis.com; wolfgang.jahnke@novartis.com

Author Contributions: **Stefan Schütz:** Conceptualization, Investigation, Resources, Formal Analysis, Visualization, Writing – Original Draft, Writing – review & editing. **Christian Bergsdorf:** Investigation, Methodology, Resources, Formal Analysis, Writing – review & editing. **Sandra Hänni-Holzinger-:** Resources, Writing – review & editing. **Andreas Lingel:** Conceptualization, Writing – review & editing. **Martin Renatus:** Conceptualization, Writing – review & editing. **Alvar D. Gossert:** Conceptualization, Supervision, Writing – review & editing. **Wolfgang Jahnke:** Conceptualization, Supervision, Writing – review & editing.

Competing Interest Statement: All authors are current or former employees of Novartis Pharma AG. S.S., C.B., S.H.-H., A.L., M.R., A.D.G., W.J. and/their spouses are shareholders of Novartis Pharma AG. M.R. is a current employee and may hold shares of Ridgeline Therapeutics. Ridgeline Therapeutics did not provide funding for this work.

Keywords: MYC, intrinsically disordered protein, E-Box, bHLH-LZ, transcription factor

ABSTRACT

The basic helix-loop-helix leucine zipper (bHLH-LZ) transcription factor (TF) MYC is an intrinsically disordered oncoprotein. In complex with its obligate heterodimerization partner MAX, MYC preferentially binds E-Box DNA sequences (CANNTG). At promotors containing these sequence motifs, MYC controls fundamental cellular processes such as cell cycle progression, metabolism, and apoptosis. A vast network of proteins controls MYC function via intermolecular interactions. In this work, we establish another layer of MYC regulation by intramolecular interactions. We use Nuclear Magnetic Resonance (NMR) spectroscopy to identify and map multiple binding sites for the C-terminal MYC:MAX DNA binding domain (DBD) on the intrinsically disordered regions (IDRs) in the MYC N-terminus. We find that these binding events in *trans* are driven by electrostatic attraction, that they have distinct affinities, and that they are competitive with DNA binding. Thereby, we observe the strongest effects for the N-terminal MYC box 0 (Mb0), a conserved motif involved in MYC transactivation and target gene induction. We prepared recombinant full-length MYC:MAX complexes and demonstrate that the interactions identified in this work are also relevant in *cis*, i.e. as intramolecular interactions. These findings are supported by Surface Plasmon Resonance (SPR) experiments, which revealed that intramolecular IDR:DBD interactions in MYC decelerate the association MYC:MAX complexes to DNA and that they provide selectivity for target E-Box sequences. Our work offers new insights how bHLH-LZ TFs are regulated by intramolecular interactions, which opens up new possibilities for drug discovery efforts.

SIGNIFICANCE STATEMENT

MYC is a key oncoprotein that is dysregulated in most human cancers. As a transcription factor, it regulates fundamental cellular processes. Consequently, MYC is tightly controlled from gene to protein, including intermolecular protein-protein interactions. In this work, we establish a so far unknown layer of MYC regulation by intramolecular interactions that occur between conserved disordered motifs in the MYC N-terminus and the basic DNA binding domain. We find that these interactions compete with DNA binding, which especially decelerates association of non-target DNA to the MYC:MAX complex, thereby providing selectivity for consensus E-Box sequences. Our newly identified intramolecular MYC interactions can be utilized for developing novel starting points for direct MYC-targeting treatments.

Main Text

Introduction

The oncoprotein MYC is upregulated in more than 70 % of human cancers, and despite decades of research there is no approved MYC-targeting treatment to date(1–3). Only one candidate, the designed MYC variant Omomyc (Omo-103), proved successful in phase I/II clinical trials so far (4). Due to its central role in many fundamental biological processes(5) such as cell growth and proliferation(6, 7), tumorigenesis(8–10) and apoptosis(11, 12), MYC needs to be tightly controlled on all possible levels from gene to protein(13–18), which involves a tight network of interacting partner proteins(19–21).

One reason why MYC is such a difficult-to-drug target is its intrinsically disordered nature (22, 23). Scattered across the N-terminal 350 amino acid-long disordered region are short conserved sequence elements, so-called MYC boxes (Mb), that serve as binding sites for transactivating factors and other interaction partners (24–28). In complex with a binding partner, these MYC boxes might adopt a defined structure, while they appear disordered in the unbound form (29). The C-terminus of MYC harbors the basic region and the helix-loop-helix motif (bHLH) followed by a leucine zipper (LZ), the latter promoting heterodimerization with other proteins of the bHLH-LZ family(30). As a dimer, the bHLH-LZ motif forms the DNA-binding domain (DBD) (31) by adopting a stable α-helical fold even in the absence of DNA. The best characterized dimerization partner of MYC is the MYC-associated factor X (MAX), a 160 amino acid protein with a bHLH-LZ motif in its central region (residues 22-102) that is flanked by disordered N- and C-terminal tails (32, 33). In contrast to MAX, which can form homodimers, MYC strictly requires heterodimerization for its DNA-binding and transcriptional acivity (34–38). MYC:MAX heterodimers preferentially bind DNA sequences that contain Enhancer box (E-Box) elements with the CACGTG hexamer as a consensus motif (39, 40). However, promiscuous binding to E-box sequences with alterations in the core hexamer has been reported as well, especially in the case of malignant MYC upregulation (41–44). While many drug discovery efforts target the MYC:MAX DBD, the high positive net charge and the shallow, poorly defined pocket between the two basic helices might impose a diffulty to directly target MYC at this particular site with low molecular weigth compounds (1, 3).

In recent years, it became evident that intriscically disordered regions (IDRs) are important for proper transcription factor (TF) function and regulation(45). However, whether the MYC IDRs have a regulatory role, in addition to binding factors involved in MYC transactivation or turnover, is an aspect that has so far not been extensively explored. In this work, we use Nuclear Magnetic Resonance (NMR) spectroscopy to identify and map interactions between MYC IDRs, as well as between Mb's and the MYC:MAX DBD. We produced full-length MYC:MAX protein in milligram scale and used Surface Plasmon Resonance (SPR) experiments to show that conserved Mb's, especially Mb0, are key determinants for the reduced DNA affinity of full-length MYC:MAX compared to the isolated DBD. SPR measurements further reveal a ten-fold higher affinity of full-length MYC:MAX to E-Box than to mutant E-Box DNA. Mb's thus provide specificity of MYC:MAX for consensus DNA sequences via a DNA-competitive mechanism.

Our work provides first evidence for direct, intramolecular Mb:DBD interactions within MYC. We find that these interactions play an important role in regulation of MYC activity and selectivity. Our results thus open up new paths to drug discovery for a direct MYC-targeting approach by utilizing the herein indentified protein-protein interactions.

Results

Preparation of full-length MYC:MAX in milligram scale

Structural and biophysical studies of full-length MYC have long been hampered by the inability to produce full-length MYC in sufficient quantity and quality. The majority of *in vitro* studies thus relied on shorter MYC constructs, that comprise either the folded C-terminal basic helix-loop-helix leucine zipper (bHLH-LZ) motif or portions of the N-terminal transactivation domain (TAD). For this study, we improved a previously published protocol(46) to enable milligram-scale preparations of full-length MYC:MAX complex from recombinant proteins expressed in *E. coli* (see Materials and Methods). Essentially, we were able to refold and purify homogenous full-length MYC:MAX at concentrations of up to 40 µM.

Disordered regions in full-length MYC reduce the DNA binding affinity of the MYC:MAX TF

When we assessed DNA binding of our reconstituted full-length MYC:MAX complex, we noticed that it exhibited a remarkably lower affinity towards E-Box DNA than what has been reported by us and others for the isolated MYC:MAX DNA binding domain (DBD)(47–50). We therefore tested three different MYC:MAX complexes, that varied in the length of the MYC protein, for their binding to a set of four different DNAs using Surface Plasmon Resonance (SPR; Fig. 1). We chose the canonical E-Box sequence (CACGTG), a negative control DNA (TTAGCA) and two mutant E-Box sequences from the literature (Fig. 1B)(43). The mutant E-Box sequences carried two mutations in the core hexamer either in the middle of the recognition site (mutant E-box 1, CATATG, referred to as “low-affinity E-Box”) or at the ends (mutant E-box 2, AACGTT, referred to as “non E-Box”), which still allow for specific recognition by MYC:MAX, albeit with weaker affinity.

We find that all three tested MYC proteins MYC(2–439), MYC(151–439) and MYC(352–437), in complex with full-length MAX, bind strongest to E-Box DNA. The affinity towards the mutant E-Box sequences was reduced (Fig. 1A), and the negative control DNA was weakly bound only by the MYC(352–437):MAX(2–160) complex. Compared to the latter, the affinity of full-length MYC:MAX is reduced for all tested DNA sequences. Notably, this reduction is larger for mutant E-boxes (more than 20-fold) than for the canonical E-Box (about 8-fold). MYC:MAX complexes with the intermediate MYC(151–439) protein show intermediate affinity reductions which are also more pronounced for mutant E-boxes (8- to >10-fold) compared to canonical E-box DNA (3-fold) (Fig. 1A). We thus conclude that the N-terminal disordered part of MYC selectively weakens the intrinsic affinity of the MYC:MAX DBD toward non-canonical, off-target DNA sequences.

Expression strategy for disordered MYC fragments

Sequence analysis of MYC and MAX proteins suggested that the observed effects on DNA binding might be attributed to interactions between the acidic disordered TAD and the basic DBD. As these would be difficult to characterize in the full-length protein, we set out to identify potential MYC:MYC interactions using a divide-and-conquer approach. Taking the established N- and C-terminal fragments MYC(1–88)(51) and MYC(352–437)(30) as a basis, we divided the remaining central part into five constructs with a length of about 50 amino acids each (Fig. 2A and B), while preserving the conserved MYC box (Mb) motifs. These constructs were expressed in large amounts in *E. coli* (1-20 mg per L culture) as cleavable fusion proteins. We found also the longer

fragments 151–255 and 256–351 to be well-behaved with regards to expression yields, solubility and stability, which enabled us to obtain NMR resonance assignments of these two constructs (SI Appendix, Fig. S4 and S5). As the isolated MYC bHLH-LZ motif is prone to aggregation, MYC(352–437) was co-expressed with its cognate parter MAX(22–102) and purified as a heterodimer to yield highly soluble protein. Together, MYC(352–437) and MAX(22–102) form the DNA-binding domain and are devoid of long unstructured stretches (SI Appendix, Fig. S1). In the following, the heterodimer MYC(352–437):MAX(22–102) is denoted as MYC:MAX DBD.

Detection and characterization of interactions within MYC

To identify interactions between the various MYC fragments, we used Nuclear Magnetic Resonance (NMR) spectroscopy. NMR is a particularly useful method for this kind of studies since it can robustly detect weak protein-protein interactions. NMR spectra of an isotope-labeled (and thus NMR-active) protein were recorded in absence and presence of an unlabeled potential binding partner. Upon binding, the chemical environment of residues in the binding site changes. This leads to perturbations of the chemical shifts of the affected nuclei and ultimately to altered positions of the respective peaks in the NMR spectrum. Conversely, the absence of chemical shift perturbations (CSPs) is an indication that two potential binding partners do not directly interact with each other, at least under the given assay conditions. We expressed the seven MYC fragments in an NMR-active (^{15}N-labeled) form and recorded ^{1}H-^{15}N correlation spectra in absence and presence of each of the six other fragments (Fig. 2C, and SI Appendix, Fig. S2 and S3). We find that the two N-terminal fragments MYC(1–88) and MYC(89–150) interact with the MYC:MAX DBD (Fig. 2E) and with MYC(303–351), which immediately precedes the DBD (Fig. 2B and C).

In addition, the central fragments MYC(151–203), (203–255) and (256–299) also bind to the MYC:MAX DBD, while the more C-terminal MYC(303–351) does not (Fig 2E). These results were consistent regardless which one of the two components under investigation was NMR-active (Fig. 2C and D). Taken together, this data clearly demonstrates binding of the MYC N-terminal fragments to the C-terminal MYC region, especially to the MYC:MAX DBD.

Mapping of interaction sites

To map the respective binding sites of MYC fragments, we used published resonance assignments for MYC(1–88) (BMRB: 26662) and the MYC:MAX DBD (BMRB: 27571) and assigned the MYC constructs 151–255 and 256–351 ourselves (BMRB 51636 and 51635; respectively). Using standard triple resonance experiments, we assigned 100% of the backbone amide chemical shifts in both constructs (SI Appendix, Fig. S5 and S6). Assignments of MYC(151–255) and MYC(256–351) could easily be transferred to the shorter fragments MYC(151–203), MYC(203–255), MYC(256–299) and MYC(303–351), as we found them to act as independent entities within the continuous polypeptide chain.

Binding of the MYC(1–88) and MYC(303–351) fragments could be mapped to an interaction between the conserved Mb0 (residues 15–32) and an extended stretch including the MbIV (residues 304–324) and the NLS (Nuclear Localization Signal, residues 320–328) (SI Appendix, Fig. S7). As we measured an affinity in the millimolar range , we did not further pursue this interaction. However, we cannot rule out that it is indeed biological meaningful.

Most MYC:MYC interactions identified in this study involve the structured MYC:MAX DBD (Fig. 2C). Except for the basic MYC(303–351), all other fragments interact with the highly positively charged MYC:MAX DBD in our NMR binding assay (Fig. 3A and Suppl. Fig 3). The interaction between MYC(1–88) and the MYC:MAX DBD is reminiscent of the binding of the disordered MAX N-terminus to the DBD that we showed previously(47). The MYC(1–88) construct is well studied with regard to MbI-dependent MYC degradation and heterotypic protein-protein interactions(15, 20, 27, 52). Chemical shift mapping revealed that within MYC(1–88) the Mb0 motif is the binding site for the DBD, while the MbI motif is not involved in the interaction (Fig. 3B). In the MYC:MAX DBD, MYC and MAX residues within the bHLH motif show significant CSPs upon binding of the isolated Mb0 peptide, while residues in the leucine zipper are not involved in binding (SI Appendix, Fig. S8). We could further support these results by paramagnetic relaxation enhancement (PRE) data. To this end, we produced recombinant MYC(11–34) (Mb0 peptide), coupled it with the TEMPO spin label on residue C25 and recorded spectra of the MYC:MAX DBD in presence of TEMPO-labeled Mb0 in the paramagnetic (oxidized) and diamagnetic (reduced) form. The free radical of the oxidized spin label results in enhanced nuclear relaxation of nearby residues, i.e. within the binding site, and consequently in reduced peak intensities. Decreased I_{ox}/I_{red} intensity ratios over a stretch of residues identifies the binding site. Our analysis showed that MYC and MAX residues especially between the basic region and helix 1 and between the loop and helix 2 experience PRE effects (SI Appendix, Fig. S8), corroborating our CSP data.

We next performed titration experiments on NMR-active MYC:MAX DBD with unlabeled Mb0 peptide (Fig. 3C and SI Appendix, Fig. S9), which revealed an affinity in the low micromolar range (K_D ~7 µM; Fig. 3D). In addition to Mb0 within MYC(1–88), we were able to map three additional interaction sites with the MYC:MAX DBD in the central MYC region using our new assignments (SI Appendix, Fig. S10). First, a region around the MbIIIa motif within MYC(151–203); second, the PEST region enriched in proline (P), glutamate (E), serine (S), and threonine (T) residues within MYC(203–256); and third, MbIIIb within MYC(256–299). These fragments exhibit affinities between 50 and 500 µM (SI Appendix, Fig. S11; Table 1). As we lack resonance assignments for MYC(89–150), we were not able to identify the residues involved in binding to the MYC:MAX DBD for this MYC fragment.

Interactions are driven by electrostatic effects

The identified DBD-binding MYC fragments have isoelectric points (pI) below 6.1 (Fig. 2B) and are, consequently, negatively charged in our NMR experiments (pH 7) and under physiological conditions. The acidic character of the MYC box motifs implies that their interactions with the MYC:MAX DBD are mainly driven by electrostatic attraction. We showed this exemplarily for binding of the DBD to Mb0 and MYC(256–299), for which we found that CSPs are reduced with increasing salt concentrations and almost completely abolished above 300 mM NaCl (Fig. 3D and SI Appendix, Fig. S12). Notably, higher salt concentrations are required to fully abrogate binding of Mb0 to the DBD, which coincides with the stronger affinity of this interaction compared to binding of MYC(256–299) to the DBD. These results support electrostatic interactions as a general mechanism for the interaction of acidic MYC fragments with the basic DBD. Indeed, the MYC and MAX bHLH-LZ motifs have high pI values of 10.1 and 9.9, respectively, whereas the interacting Mb0, MbIIIa and MbIIIb motifs have low, but comparable pI values of 3.3, 3.4 and 4.3. Nevertheless, we measure binding affinities that differ by almost two orders of magnitude, ranging from single-digit to several hundred micromolar for the Mb0 and the MbIIIb-containing

MYC fragment, respectively (Fig. 3D and SI Appendix, Fig. S11). We thus conclude that other, more specific interactions based on amino acid composition or (transient) structural elements might contribute to binding as well.

Intramolecular backfolding and DNA binding are mutually exclusive

Previously, we showed that the disordered, acidic MAX N-terminus binds to the MYC:MAX DBD in a DNA-competitive manner(47). We thus anticipated that binding of the acidic MYC fragments to the DBD also directly competes with DNA binding. To this end, we performed competition experiments by NMR with MYC:MAX DBD, DNA and recombinant Mb0 peptide (MYC(11–34)) or MYC(256–299). For the former, we coupled an NMR-active ^{13}C-labeled methyl group to a reactive cysteine (C25) via a disulfide linkage. The resulting S-^{13}C-methylthiocysteine (^{13}C-MTC) has been shown to possess favorbale NMR properties for structural and functional studies, even for large proteins and complexes(53). Both Mb0(^{13}C-MTC-25) and ^{15}N-labeled MYC(256–299) do not bind isolated E-Box DNA, but they clearly interact with the MYC:MAX DBD, resulting in CSPs between the free and the bound state (Fig. 4A, SI Appendix, Fig. S12A). However, in presence of MYC:MAX DBD and E-Box DNA, resonances of the peptides appear close to or at the same chemical shift as for the free peptides, indicating displacement of the peptides from DBD by the DNA. For MYC(259–299), this was achieved by equimolar addition of DNA (SI Appendix, Fig. S13A), while for the Mb0 peptide a 5-fold excess of DNA was required to obtain full displacement (Fig. 4A). This is in line with the higher affinity of the Mb0 for the DBD as that of MYC(256–299) (Table 1). These results argue that in presence of saturating amounts of E-Box DNA, the MYC:MAX DBD can no longer interact in *trans* with the MYC boxes, likely because binding sites in the DBD are occupied by DNA, and, consequently, the MYC fragments appear as free proteins.

Based on these experiments, which assessed the DNA-competitive interaction of MYC box motifs and the DBD in *trans*, i.e. as an intermolecular interaction, we aimed for an experimental setup to confirm the observed effect in an intramolecular setting. To this end, we designed MYC:MAX complexes, where we artifically fused the Mb0, MbIIIa or MbIIIb peptides directly to the MYC bHLH-LZ motif (Fig. 4B and SI Appendix, Fig. S13B). A short linker between the motifs ensures sufficient mobility of the peptides to engage in binding to the DBD. We then compared these constructs with MYC(352–437):MAX(2–160), that lacks any DBD-interacting MYC box, in our SPR assay using E-Box and mutant E-Box 2 DNA (Fig. 4B-D, SI Appendix, Fig. S14). We found that the Mb0 has the largest effects, both on reducing overall affinity for DNA and on providing selectivity for the consensus E-Box (Fig. 4C and D). The effects for the MbIIIa- and MbIIIb-linked MYC:MAX DBDs were less pronounced, which coincides with the lower affinities that we measured for binding of the MbIIIa- and MbIIIb-containing MYC fragments to the MYC:MAX DBD compared to the high affinity for binding of Mb0 to the DBD (Table 1).

Conquer full-length MYC:MAX by NMR

Finally, we attempted to demonstrate intramolecular backfolding of MYC box motifs to the DBD by NMR in the native, full-length proteins. The long unstructured regions in MYC, but also in MAX (SI Appendix, Fig. S1), pose a severe difficulty for structural studies. In addition, the size of the full-length MYC:MAX complex of about 66.5 kDa and the combination of both disordered regions and folded parts make it challenging for NMR. In initial attempts to make full-length MYC:MAX amenable for NMR, we refolded uniformly ^{13}C- and ^{15}N- labeled MAX with unlabeled MYC. However, we only observed resonances that correspond to the disordered MAX C-terminus, while

resonances for the MAX bHLH-LZ were not detectable. This is likely due to line broadening stemming from unfavorable relaxation mechanisms in the full-length protein complex.

We thus turned to post-translational isotope labeling and employed the ^{13}C-MTC appproach used earlier for the Mb0. We designed a "Cys-light" MYC construct, in which all cysteine residues except C25 were mutated to alanine (MYC(2–439_C0, C25)), reconstituted dimers with full-length MAX, and incubated the complexes with ^{13}C-MMTS (^{13}C-methyl methanethio-sulfonate). As MAX is devoid of any cysteine, we achieved 100% labeling on the single remaining Cys25 (^{13}C-MTC-25) in the Cys-light MYC without any side reaction.

In addition, we similarly labeled the Mb0-MYC(352–437):MAX(2–160) construct. As expected, methyl-TROSY spectra of the two ^{13}C-MTC-labeled MYC:MAX complexes display a single peak (Fig. 4E and F), that showed CSPs upon addition of E-Box DNA. Strikingly, the peak shifts are accompanied by a strong increase in peak intensity (compare 1D cross-sections through the peaks in both ^{1}H and ^{13}C). We attribute this observation to a order-to-disorder transition of the ^{13}C-MTC-labeled Mb0 from a relatively rigid DBD-bound form in the absence of DNA to a more flexible unbound form in presence of DNA, i.e. when DNA displaces Mb0 from the DBD binding site. In the latter case, the Mb0 behaves more like a free, small disordered peptide resulting in faster tumbling and increased peak intensity, although it is still tethered to the rest of the MYC protein in the large MYC:MAX complex.

Additionally, we could displace DBD-bound Mb0 in a concentration dependent manner with excess of MAX N-terminal peptide. The pS2, pS11 double-phosphorylation on the MAX N-terminus has recently been shown to increase its intrinsic affinity for the MYC:MAX DBD(47). We thus assumed competition of the MAX N-terminus and the Mb0 for the same DBD binding site and performed the NMR competition experiment with phosphorylated MAX(2–21). Indeed, we observed concentration-dependent CSPs and peak intensity increases for the ^{13}C-MTC-labeled Mb0-MYC:MAX complex upon addition of phosphorylated MAX(2–21) (SI Appendix, Fig. 13C). Expectedly, competition can also be achieved with excess of free Mb0 peptide. For these experiments we used a Mb0 peptide, whose reactive Cys25 thiol was blocked by alkylation with iodoacetamide to prohibit disulfide shuffling between the free and the DBD-linked, ^{13}C-MTC-labeled Mb0 (SI Appendix, Fig. 13D). We thus conclude that E-Box DNA as well as high-affinity DBD-interacting motifs in MYC and MAX efficiently compete for the same binding site on the DBD, also in context of native, full-length MYC:MAX.

All in all, we could showcase that challenging proteins such as the large and mainly disordered transcription factor complex MYC:MAX are amenable to NMR studies. Our NMR results on full-length MYC:MAX corroborate our mechanistic SPR studies and NMR experiments on isolated MYC fragments. Together, this data suggests intramolecular backfolding of the N-terminal and central MYC box motifs onto the C-terminal DBD, although they are separated by up to 300 amino acids in the native MYC protein. This backfolding mechanism is probably relevant for fine-tuning DNA binding and selectivity towards E-box versus mutant E-box DNA as well as heterotypic protein-protein interactions in cellular settings, thereby providing an additional layer of transcriptional regulation.

Discussion

Electrostatic interactions drive IDR:DBD binding in the MYC:MAX complex

In this study, we identified and mapped interactions within the intrinsically disordered transcription factor MYC. Thereby, we not only observe interactions between intrinsically disordered regions (IDRs) but also between IDRs and the folded DNA binding domain (DBD) that is formed by heterodimerization of the MYC and MAX bHLH-LZ motifs. In a cellular setting, these interactions can occur intramolecularly in a single MYC protein (in *cis*) or intermolecularly between two MYC molecules (in *trans*). We will discuss first the intermolecular aspect before turning to the consequences of intramolecular binding.

Closer examination of the interacting motifs indicates that the observed binding events are mainly driven by electrostatic attraction between the positively charged (basic) DBD and negatively charged (acidic) IDRs. Our findings for MYC are reminescent of other transcription factors, for which intramolecular interactions between IDRs and DBDs have been reported in the past. These include the p53 family(54), bZIP (CCAAT/ Enhancer-binding proteins, C/EBPs)(55), bHLH-LZ TFs(47) and Forkhead box (FOX) TFs(56, 57). Notably, the IDRs in p53, FOXO3a, FOXO4 and MAX have low isoelectric points of 3.3, 3.4, 2.9 and 3.6, which renders these regions negatively charged under physiological conditions and thus enables interactions with their respective DBDs (pI values of 8.9, 10.5, and 9.6 for p53, FOXO and MAX). The results that we present in this study for MYC support electrostatics-driven interactions between acidic disordered regions and basic DBDs as an important and common regulatory mechanism that is shared among different TF families.

Albeit electrostatic interactions are important for interactions in MYC, we notice pronounced differences in the affinities of these binding events. In essence, we measured affinities in *trans* that cover a range of about three orders of magnitude (Table 1). Thereby, the weakest interaction is between the disordered fragments MYC(1–88) and MYC(303–351) with a K_D in the low millimolar range. The affinities for the MbIIIa- and MbIIIb-containing fragments MYC(151–203) and MYC(256–299) to the MYC:MAX DBD are in the high micromolar range, while we find the PEST sequence and the Mb0 to interact with the DBD with double- and single-digit micromolar affinity, respectively (Table 1). Interestingly, the nuclear concentration of MYC was reported to be up to several micromolar, depending on cell stimulus and without consideration of sub-nuclear compartmentalization(58). Consequently, at least the strong affinities between that we measured are in the range of physiological MYC concentrations. Moreover, the design of our NMR binding experiments was such that the interactions were in *trans*, while in native full-length MYC these would be intramolecular interactions. We and others have shown that weak intermolecular binding events become significantly more affin and efficient when they become intramolecular interactions(47, 59, 60). We conclude that the interactions found in this study, especially between disordered MYC fragments and the folded DBD, are biologically meaningful.

The interplay of weak but multivalent intermolecular interactions between IDRs or between IDRs and folded domains, as we described for MYC (this study) and previously for MAX(47), is reminescent of processes that manifest as LLPS *in vitro* and *in vivo*(61, 62). Members of the bHLH-LZ family, among them MYC as a prominent example, contain regions with the predicted potential to drive phase separation(23). Indeed, c-MYC has been shown to undergo homotypic LLPS and molecular determinants for this process have been dissected in more detail(63, 64). Additionally, LLPS-mediated target gene activtion has been demonstrated for the TFs OCT4 and GCN4(63),

TAZ/TEAD(65), engineered OptoDroplet TFs(66), and N-MYC(67). Weather the herein identified MYC:MYC interactions contribute to transcriptionally active foci also for c-MYC has to be shown in future studies.

Kinetic parameters establish a mechanistic model of DNA binding by the MYC:MAX TF

We used SPR as a first step to shed light on the biological relevance of the identified MYC:MYC interactions, as it allowed us to screen MYC proteins of variable length ranging from the bHLH-LZ to the full-length protein. Since the quantitative assessment of kinetic DNA binding parameters (k_{on} and k_{off}) was not possible for all the different MYC:MAX complexes used in this work, we restrict our discussion to a qualitative comparison.

Importantly, we find that the disordered regions in MYC provide selectivity for canonical E-Box DNA over mutant E-Boxes or random DNA sequences (Fig. 1). A visual inspection of the SPR sensorgrams revealed that the affinitiy differences observed between the MYC:MAX DBD and full-length MYC:MAX are due to considerably slower association rates for the latter (Fig. 1C). By contrast, the dissociation rates are comparable for both complexes.

Based on our NMR and SPR data, we propose the following model of DNA engagement by the full-length MYC:MAX complex: a DNA-free MYC:MAX complex, as it would appear for example after translation in the cytosol, adopts a "locked" state, where a MYC box (e.g. Mb0) folds back to the DBD, creating a conformational situation that is reminescent of DNA binding (Fig. 5A). Once in the nucleus, DNA would have to compete with the MYC box that occupies the DBD. As a consequence, this competition slows down association of the DNA to MYC:MAX, since the MYC box has to dissociate first. The MYC box, that is now released from the DBD, is separated from the binding site by a relatively long linker, making it stochastically less likely to engange in productive encounters with a DNA-bound DBD. Consequently, full-length MYC:MAX has comparable dissociation rates as MYC(352–437):MAX(2–160) – in both complexes the dissociation from DNA is driven by the proximal MAX N-terminus that has an intermolecular K_D of 13.2 µM for the DBD (<< 5 µM when double-phosphorylated) and is attached to it via a very short linker(47).

These considerations are supported by our SPR data for the artificial Mb-linked MYC:MAX complexes. When we tethered additional DBD-interacting motifs (i.e. Mb0, MbIIIa or MbIIIb) to MYC:MAX via short linkers (Fig. 4B and SI Appendix, Fig. S13B), we observed accelerated dissociation from DNA for these complexes compared to MYC(352–437):MAX(2–160), while the association rates were similar (Fig. 4C), as concluded from a qualitative evaluation of the SPR sensorgrams.

We rationalize this change from dissociation rate-driven affinity reduction as observed for Mb-linked MYC:MAX to association rate-driven affinity reduction as observed for full-length MYC:MAX with (1) the longer "spacers" between the MYC box motifs and the DBD in the full-length protein and (2) a redundancy in the Mb:DBD interactions. In full-length MYC, a DBD-interacting MYC box can easily be displaced intramolecularly by another one. Hence, DNA has to compete not only with one component but many, which slows down the binding process of the DNA to the DBD. This redundancy would further ensure that the selectivity for target gene promotors (containing the canonical E-Box recognition sequence) is maintained in case a particular MYC box is temporarily enganged in intermolecular interactions with other MYC binding proteins.

New avenues for MYC targeting in drug discovery

Capitalizing on the herein identified and characterized interactions could provide new starting points for the identification of novel modalities to directly target MYC in drug discovery. Low molecular weight compounds could act as molecular glues that strengthen the Mb0:DBD interaction and lock MYC in a conformation that is less efficient in DNA binding (Fig. 5B). Eventually, covalent approaches can even utilize the reactive Cys25 in Mb0. Our NMR data with unmodified, ^{13}C-MTC-, acetamide- and TEMPO-labeled Mb0 suggests that the DBD in principal tolerates covalent modifications on Cys25 (SI Appendix, Fig. S15). Although the mentioned modifications weaken the Mb0:DBD interaction to some extent, structure-guided medicinal chemistry efforts might be able to pick up favorable interactions, which could increase the affinity. Ultimately, these efforts would result in a "locked" MYC:MAX whose DNA binding, especially to off-target sequences, is further reduced, thereby lowering the oncogenic potential of MYC.

Materials and Methods

Protein expression

All genes were codon optimized for expression in E.coli and cloned into modified pET vectors. MYC (UniProt P01106) 1–88, 89–150, 151–203, 203–255, 256–299, 303–351, 151–255 and 256–351 fragments carry an N-terminal His6-ZZ-TEV tag. Full-length MYC(1–439) and MYC(1–439_C70A, C117A, C133A, C171A, C188A, C208, C300A, C342A, C438A), short MYC(1–439)_C0,C25, were cloned without any purification tag. MYC(11–34), corresponding to the Mb0 peptide, carries an N-terminal His6-MBP-TEV tag. MAX(2–160) carried an N-terminal TEV-cleavable Strep-tag. MYC:MAX DBD complexes were cloned with an uncleavable His6-tag on MYC. Mb0-MYC:MAX DBD, MbIIIa-MYC:MAX DBD and MbIIIb-MYC:MAX DBD constructs carried a TEV-cleavable His6-tag. Molecular cloning and site-directed mutagenesis were performed with an adapted strategy based on the Golden Gate Assembly method using Type IIS restriction enzymes(68). See SI Appendix, Table S2 for a comprehensive list of protein constructs used in this study.

Escherichia coli BL21 (DE3) cells (#C2527, NEB) were transformed with the appropriate plasmid and grown at 37°C to an OD_{600} of 0.8 - 1.0 in MOPS-buffered Terrific broth (TB). Overexpression of soluble proteins was induced with 0.2 - 0.5 mM IPTG at 20°C. After 15h, cells were harvested by centrifugation. Overexpression of full-length MYC into inclusion bodies was induced with 1 mM IPTG and cells were maintained at 37 °C for 5h before harvest. Proteins with stable isotopic labeling for NMR studies were obtained by overexpression in M9 minimal medium that was supplemented with 1 g/L $^{15}NH_4Cl$ as the sole nitrogen source and 4 g/L D-glucose or 2 g/L $^{13}C_6$-glucose as the sole carbon source. For labeling of the MYC:MAX DBD, the M9 medium was based on D_2O.

Purification of soluble proteins

Cells were resuspended in buffer A (50 mM Tris, pH 8, 300 mM NaCl, 1 mM DTT) complemented with 10 mM imidazole, lysozyme, 0.1 % (v/v) Triton X-100, 5 mM $MgCl_2$ and 25 U/mL Turbonuclease. For ZZ- or MBP-tagged MYC constructs, cell lysis was performed by sonication on ice, while for cells containing full-length MYC, MYC:MAX complexes or MAX(2–160) a high-pressure homogenizer was used. The lysate was cleared by centrifugation.

For His-tagged MYC proteins, the supernatant was loaded on 5 mL pre-packed Ni-NTA columns. The resin was washed with 20 CV (column volumes) buffer A mixed with 1 % buffer B (as buffer A, supplemented with 1 M imidazole). The resin-bound protein was eluted with a gradient of 5-30 % buffer B over 20 CV, followed by a gradient from 30-100% buffer B over 4 CV. Eluted proteins with cleavable His-tag were supplemented with TEV protease and dialyzed at 4 °C overnight against buffer C (20 mM HEPES, pH 7.3, 100 mM NaCl, 2 mM DTT). Dialysates were cleared from precipitate by filtration and applied to 5 mL Ni-NTA resin in a gravity flow column equilibrated with buffer D (20 mM HEPES, pH 7.3, 500 mM NaCl, 1 mM DTT) supplemented with 10 mM imidazole. The column was washed with 3 CV buffer D supplemented with 20 mM imidazole. The resin-bound purification tag was eluted with 5 CV buffer B. Fractions containing the cleaved target protein were further purified by size exclusion chromatography (SEC). SEC was performed on HiLoad 16/600 Superdex 75 columns (Cytiva) in buffer E100 (20 mM HEPES, pH 7, 100 mM NaCl, 2 mM TCEP).

For MYC:MAX DBD complexes, buffers A and B were additionally supplemented with 10 % (v/v) glycerol. After elution from the IMAC resin, the NaCl concentration was reduced to 200 mM by dilution with 0.5 Vol H_2O. The diluted complexes were further purified on a 5 mL HiTrap Heparin column (Cytiva) equilibrated in buffer F (25 mM Tris, pH 8, 200 mM NaCl). The target proteins were separated from DNA and contaminants via a 10 CV wash step with 10 % buffer G (25 mM Tris, pH 8, 2 M NaCl), followed by a gradient from 10-50 % buffer G over 40 CV and 50-100 % buffer G over 4 CV. Fractions containing MYC:MAX complexes were pooled and purified to homogeneity via SEC as above. MAX(2–160) was purified as described before(47).

For the Mb0 peptide that carries a TEV-cleavable MBP-tag the dialysis step after elution from the IMAC resin was omitted. The TEV-cleaved peptide was directly subjected to SEC (HiLoad 16/600 Superdex 30, Cytiva) in 50 mM NH_4HCO_3. Fractions containing the target peptide were pooled, flash-frozen in liquid nitrogen and lyophilized. Dry peptide was dissolved in 100% d_6-DMSO to a final concentration of 10 or 20 mM.

Purification of full-length MYC from inclusion bodies

Cells from 2 L culture were resuspended in 50 mL cold IB buffer (50 mM Tris, pH 8, 5 mM EDTA, 5 mM Benzamidine, 1 mM DTT) complemented with lysozyme, 5 mM $MgCl_2$, 25 U/mL Turbonuclease and complete protease inhibitor cocktail (Roche). After cell lysis, the inclusion body pellet was washed with 30 mL IB buffer followed by a wash with 30 mL water. Afterwards, the pellets were dissolved in buffer U7 (7 M Urea, 25 mM HEPES, pH 7.6, 300 mM NaCl, 15 % v/v glycerol, 1 mM DTT, 0.1 mM EDTA) supplemented with complete protease inhibitor cocktail (Roche) to a protein concentration of about 5 mg/mL. Any insoluble debris were removed by centrifugation. The supernatant was flash-frozen in aliquots and stored at -80 °C. Typically, at this step more than 50 mg protein were obtained from 1 L expression medium. LC-MS analysis

confirmed cleavage of the N-terminal methionine stemming from the translation start site, resulting in MYC(2–439).

Refolding of full-length MYC:MAX

Full-length MYC:MAX complexes were reconstituted by diluting equimolar amounts of MYC(2–439) and MAX(2–160) into buffer U6 (as U7, but with 6M urea) to a final concentration of 0.25-0.3 mg/mL. We typically refold 25-30 mg MYC with an appropriate amount of MAX, corresponding to not more than 0.5 L expression volume for each of the two proteins. MYC:MAX complexes were refolded by rapid, stepwise dialysis. Dilute MYC:MAX solution in buffer U6 was transferred to a dialysis bag with 12-14 kDa MWCO (SpectraPor) and dialyzed for 1 h at 20 °C against 2 L buffer U3 (as U7, but with 3 M urea), followed by dialysis for 1 h at 20 °C against 2 L buffer U1 (as U7, but with 1 M urea), for 1 h at 20 °C against 3 L buffer U.5 (as U7, but with 0.5 M urea), and finally overnight at 4 °C against 4 L buffer U0 (as U7, but without urea). Refolded MYC:MAX was further purified via ion exchange on a pre-packed 5 mL HiTrap Heparin column (Cytiva) equilibrated in buffer F. The column was washed with 5 CV buffer F and MYC:MAX was eluted with a steep gradient from 0 to 100% buffer G over 10 CV, followed by 5 CV 100% buffer G. Fractions containing full-length MYC:MAX were pooled and concentrated in Amicon Ultra-15 centrifugal filters with 10 kDa MWCO (Millipore) to 3 mL. Final purification to homogeneity was achieved on a HiLoad 16/600 S75 column (Cytiva) in buffer E300 (20 mM HEPES, pH 7, 300 mM NaCl) supplemented with 2 mM TCEP. Fractions of 0.5 mL were collected and only four to five fractions at the elution peak maximum were pooled, flash-frozen and used in subsequent experiments without further concentration.

^{13}C-MMTS, Iodoacetamide and TEMPO spin labeling

Labeling of refolded full-length MYC:MAX with ^{13}C-MMTS (^{13}C-methyl methanethiosulfonate; Sigma-Aldrich) was performed after elution from the Heparin column (see above). Purified Mb0-MYC(352–437):MAX(2–160) was labeled after exchanging the buffer to TCEP-free buffer E100. Fully reduced Mb0 peptide was prepared by diluting a 10 mM solution of MYC(11–34) in 100% d_6-DMSO by about 100-fold in buffer E100 supplemented with 5 mM DTT, followed by buffer exchange to TCEP-free buffer E100 in a centrifugal filter (3 kDa MWCO). Proteins were incubated with a 2-fold molar excess of ^{13}C-MMTS (100 mM stock in 100% d_6-DMSO) at 4 °C overnight (ON). Acetamide-labeling was achieved by addition of a 4.5-fold molar excess of iodoacetamide (Sigma-Aldrich; 50 mM stock in 100% d_6-DMSO) and the labeling reaction was incubated ON at 4 °C in the dark. TEMPO-labeling was performed with a 10-fold molar excess of 4-maleimido-TEMPO (4-Maleimido-2,2,6,6-tetramethyl-1-piperidinyloxy; Sigma-Aldrich; 200 mM stock in 100% d_6-DMSO) and the peptide was incubated ON at room temperature in the dark. Unreacted label and side products were removed via SEC as described above, maintaining buffer conditions that are free of reducing agents. LC-MS confirmed the completeness of the labeling reaction without any secondary site labeling on MYC or MAX.

Proteins, Peptides and DNA from commercial sources

MYC(151–439):MAX(2-160) was purchased from Biortus (Jiangyin, China).

MAX(2–21)_pS2,pS11 (Ac-pSDNDDIEVEpSDEEQPRFQpSA-NH_2) was purchased from Biosyntan (Berlin, Germany). Ac- denotes an acetylated N-terminus and -NH_2 denotes an C-terminal amide, while pS is for phospho-serine.

Duplex DNA probes for SPR and NMR measurements were purchased from IDT (Leuven, Belgium). See SI Appendix, Table S1 for a complete list of DNA duplexes used in this study.

NMR spectroscopy and data analysis

All NMR samples were prepared in buffer E100 or E300 and contained 5% (v/v) D_2O. NMR spectra were recorded at 283 K for the disordered MYC fragments and at 298 K for MYC:MAX complexes on Bruker AVIII-600 and AVIII-800 spectrometers with cryogenic probe-heads. For MYC:MAX complexes, transverse-relaxation optimized spectroscopy (TROSY) techniques were employed together with deuteration to reduce relaxation(69). Backbone and side-chain resonances were assigned using standard triple-resonance CBCANH, CBCA(CO)NH, HNCO, HN(CA)CO and (H)CC(CO)NH experiments(70). Samples for assignment purposes contained 665 µM and 900 µM protein for MYC(151–255) and MYC(256–351), respectively. Several low-intensity resonances could be linked to *cis*-prolines, which were readily identified based on their characteristic Cβ, Cγ and C' chemical shifts(71).

NMR binding experiments were performed with 25 or 50 µM NMR-active protein and unlabeled protein or DNA as indicated in the figures. Heteronuclear single quantum correlation spectroscopy (HSQC) experiments were used to monitor changes in the amide proton and nitrogen chemical shifts. The combined chemical shift difference $\Delta\delta_{comb}$ of a given resonance in absence and presence of a binding partner was calculated using equation (1):

$$(1)\quad \Delta\delta_{comb} = \sqrt{{\Delta\delta_{NH}}^2 + \frac{{\Delta\delta_N}^2}{6.5}}$$

where $\Delta\delta_{NH}$ and $\Delta\delta_N$ are the differences in the amide proton and nitrogen chemical shift, which are weighted by a scaling factor R_{scale} = 6.5 (72).

Significant CSPs were determined by calculating a cut-off of 2σ from the trimmed mean(73). For intensity analysis, the ratio of peak intensities in HSQC spectra of bound (I_{bound}) and free (I_{free}) protein was calculated as I_{bound}/I_{free}.

NMR titration data was fitted globally in Origin Pro 2021 (OriginLab) using equation (2):

$$(2)\quad \Delta\delta_{comb} = \frac{\Delta\delta_{max}}{2P} \cdot \left((P + L + K_D) - \sqrt{(P + L + K_D)^2 - 4PL}\,\right)$$

where P and L are the constant protein and variable ligand concentrations, respectively, $\Delta\delta_{comb}$ is the observed chemical shift difference calculated from equation (1) and $\Delta\delta_{max}$ is the maximal chemical shift difference reached at saturation(74).

NMR experiments with ^{13}C-MTC- and TEMPO-labeled protein were carried out in buffer E100 or E300 lacking TCEP. A MYC:MAX DBD NMR sample was prepared with an equimolar amount of

TEMPO-labeled Mb0 and measured under oxidizing conditions. Subsequently, 500 µM ascorbic acid were added to the NMR sample and the measurement was repeated under reducing conditions. A control sample contained only MYC:MAX DBD and 500 µM ascorbic acid, to rule out interactions of ascorbic acid with the DBD. The ratio of peak intensities in ^{1}H-^{15}N TROSY spectra recorded under oxidizing (I_{OX}) and reducing (I_{RED}) conditions was calculated as I_{OX}/I_{RED}.

All NMR data was processed in Topspin 3.2 or 4.1 (Bruker). CCPN 3.0 (75) was used for analysis and visualization of NMR data and Pymol (pymol.org) was used to produce figures of protein structures. Backbone resonance assignments for MYC(151–255) and MYC(256–351) have been deposited in the BMRB under accession codes 51636 and 51635, respectively.

SPR

Surface plasmon resonance (SPR) experiments were performed on a Biacore 8K^{+} instrument (Cytiva). Biotinylated DNA duplexes were immobilized (up to 100 RU) on a CM4 chip which has been coated with neutravidin via amine-coupling (approx. 2000 RU). Protein samples were diluted into SPR buffer (25 mM HEPES, pH 8, 150 mM NaCl, 1 mM TCEP, 0.01 % Tween-20, 3 mM EDTA). Protein solutions (typically ranging from 0.49 nM up to 1000 nM) were applied to the flow cell at a flow rate of 75 µL/min and association was monitored for 160 s. Subsequently, dissociation in SPR buffer was monitored for 190 s. For equilibrium fits, the average response signal between 150 s and 155 s association time is considered. K_D values were fitted to a 1:1 binding model using a Hill equation:

$$(3)\quad R_{eq} = \frac{R_{max} \cdot x^n}{{K_D}^n \cdot x^n},$$

where R_{eq} is the equilibrium response signal at a given protein concentration x, R_{max} is the maximum response signal, and n is the Hill coefficient that is invariantly set to 1 during the fitting procedure. R_{eq} values were finally normalized using R_{max} to obtain values for “fraction bound”.

Acknowledgments

We thank César Fernandez for assistance with NMR experiment setup and analysis and Christelle Henry for maintenance of the NMR infrastructure. We would also like to thank Felix Freuler and Simon Hänni for excellent molecular biology support.

References

1. J. R. Whitfield, M. E. Beaulieu, L. Soucek, Strategies to inhibit Myc and their clinical applicability. *Front Cell Dev Biol* **5** (2017).

2. N. Meyer, L. Z. Penn, Reflecting on 25 years with MYC_Meyer_NatRevCancer_2008. *Nature Cancer Reviews* **8**, 976–990 (2008).

3. S. K. Madden, A. D. de Araujo, M. Gerhardt, D. P. Fairlie, J. M. Mason, Taking the Myc out of cancer: toward therapeutic strategies to directly inhibit c-Myc. *Mol Cancer* **20** (2021).

4. J. R. Whitfield, L. Soucek, The long journey to bring a myc inhibitor to the clinic. *Journal of Cell Biology* **220** (2021).

5. S. Adhikary, M. Eilers, Transcriptional regulation and transformation by Myc proteins. *Nat Rev Mol Cell Biol* **6**, 635–645 (2005).

6. E. v Schmidt, The role of c-myc in cellular growth control. *Oncogene* **18**, 2988–2996 (1998).

7. M. Eilers, Control of Cell Proliferation by Myc Family Genes. *Mol. Cells* **9**, 1–6 (1999).

8. S. Pelengaris, M. Khan, G. I. Evan, Suppression of Myc-Induced Apoptosis in Cells Exposes Multiple Oncogenic Properties of Myc and Triggers Carcinogenic Progression. *Cell* **109**, 321–334 (2002).

9. A. Sabò, *et al.*, Selective transcriptional regulation by Myc in cellular growth control and lymphomagenesis. *Nature* **511**, 488–492 (2014).

10. C. Wang, *et al.*, Long noncoding RNA EMS connects c-Myc to cell cycle control and tumorigenesis. *Proc Natl Acad Sci U S A* **116**, 14620–14629 (2019).

11. B. Amati, T. D. Littlewood, G. I. Evan, H. Land, The c-Myc protein induces cell cycle progression and apoptosis through dimerization with Max. *EMBO J* **12**, 5083–5087 (1993).

12. Q. Zhang, *et al.*, Domain-specific c-Myc ubiquitylation controls c-Myc transcriptional and apoptotic activity. *Proc Natl Acad Sci U S A* **110**, 978–983 (2013).

13. R. Sears, *et al.*, Multiple Ras-dependent phosphorylation pathways regulate Myc protein stability. *Genes Dev* **14**, 2501–2514 (2000).

14. Y. Chen, X. X. Sun, R. C. Sears, M. S. Dai, Writing and erasing MYC ubiquitination and SUMOylation. *Genes Dis* **6**, 359–371 (2019).

15. M. Yada, *et al.*, Phosphorylation-dependent degradation of c-Myc is mediated by the F-box protein Fbw7. *EMBO Journal* **23**, 2116–2125 (2004).

16. C. V. Dang, MYC on the path to cancer. *Cell* **149**, 22–35 (2012).

17. M. Sachdeva, *et al.*, p53 represses c-Myc through induction of the tumor suppressor miR-145. *Proc Natl Acad Sci U S A* **106**, 3207–3212 (2009).

18. D. Levens, You don't muck with MYC. *Genes Cancer* **1**, 547–554 (2010).

19. C. Grandori, S. M. Cowley, L. P. James, R. N. Eisenman, The MYC/MAX/MAD network and the transcriptional control of cell behavior. *Annu. Rev. Cell Dev. Biol* **16**, 653–99 (2000).

20. M. Kalkat, *et al.*, MYC Protein Interactome Profiling Reveals Functionally Distinct Regions that Cooperate to Drive Tumorigenesis. *Mol Cell* **72**, 836-848.e7 (2018).

21. W. B. Tu, *et al.*, Myc and its interactors take shape. *Biochim Biophys Acta Gene Regul Mech*, 469–483 (2015).

22. J. Jumper, *et al.*, Highly accurate protein structure prediction with AlphaFold. *Nature* **596**, 583–589 (2021).

23. A. Tarczewska, B. Greb-Markiewicz, The significance of the intrinsically disordered regions for the functions of the bHLH transcription factors. *Int J Mol Sci* **20** (2019).

24. M. E. Beaulieu, F. Castillo, L. Soucek, Structural and Biophysical Insights into the Function of the Intrinsically Disordered Myc Oncoprotein. *Cells* **9**, 1038 (2020).

25. Q. Zhang, *et al.*, MB0 and MBI are independent and distinct transactivation domains in MYC that are essential for transformation. *Genes (Basel)* **8** (2017).

26. A. Huang, *et al.*, "Identification of a Novel c-Myc Protein Interactor, JPO2, with Transforming Activity in Medulloblastoma Cells" (2005).

27. S. Helander, *et al.*, Pre-Anchoring of Pin1 to Unphosphorylated c-Myc in a Fuzzy Complex Regulates c-Myc Activity. *Structure* **23**, 2267–2279 (2015).

28. E. J. Feris, J. W. Hinds, M. D. Cole, Formation of a structurally-stable conformation by the intrinsically disordered MYC:TRRAP complex. *PLoS One* **14** (2019).

29. E. M. Blackwood, R. N. Eisenman, Max: A Helix-Loop-Helix Zipper Protein That Forms a Sequence-Specific DNA-Binding Complex with Myc. *Science (1979)* **251**, 1211–1217 (1991).

30. S. K. Nair, S. K. Burley, X-Ray Structures of Myc-Max and Mad-Max Recognizing DNA: Molecular Bases of Regulation by Proto-Oncogenic Transcription Factors. *Cell* **112**, 193–205 (2003).

31. S. Sammak, *et al.*, Crystal Structures and Nuclear Magnetic Resonance Studies of the Apo Form of the c-MYC:MAX bHLHZip Complex Reveal a Helical Basic Region in the Absence of DNA. *Biochemistry* **58**, 3144–3154 (2019).

32. G. J. Kato, W. M. F. Lee, L. Chen, C. v Dang, "Max: functional domains and interaction with c-Myc" (1992).

33. J. F. Naud, *et al.*, Structural and thermodynamical characterization of the complete p21 gene product of Max. *Biochemistry* **44**, 12746–12758 (2005).

34. F. O. McDuff, J. F. Naud, M. Montagne, S. Sauvé, P. Lavigne, The Max homodimeric b-HLH-LZ significantly interferes with the specific heterodimerization between the c-Myc and Max b-HLH-LZ in absence of DNA: A quantitative analysis. *Journal of Molecular Recognition* **22**, 261–269 (2009).

35. P. Lavigne, *et al.*, Insights into the Mechanism of Heterodimerization from the 1 H-NMR Solution Structure of the c-Myc-Max Heterodimeric Leucine Zipper. *J Mol Biol* **281**, 165–181 (1998).

36. J. Hu, A. Banerjee, D. J. Goss, Assembly of b/HLH/z proteins c-Myc, Max, and Mad1 with cognate DNA: Importance of protein-protein and protein-DNA interactions. *Biochemistry* **44**, 11855–11863 (2005).

37. A. R. Ferré-D'Amare, G. C. Prendergast, E. B. Ziff, S. K. Burley, Recognition by Max of its cognate DNA through a dimeric b/HLH/Z domain. *Nature* **363**, 38–45 (1993).

38. A. v. Grinberg, C.-D. Hu, T. K. Kerppola, Visualization of Myc/Max/Mad Family Dimers and the Competition for Dimerization in Living Cells. *Mol Cell Biol* **24**, 4294–4308 (2004).

39. T. K. Blackwell, L. Kretzner, E. M. Blackwood, R. N. Eisenman, H. Weintraub, Sequence-Specific DNA Binding by the c-Myc Protein. *Science (1979)* **250**, 1149–1151 (1990).

40. E. Kerkhoff, K. Bister, K.-H. Klempnauer, Sequence-specific DNA binding by Myc proteins. *Proc. Natl. Acad. Sci. USA* **88**, 4323–4327 (1991).

41. D. L. C. Solomon, B. Amati, H. Land, "Distinct DNA binding preferences for the c-Myc/Max and Max/Max dimers" (1993).

42. E. v Prochownik, M. E. Vanantwerp, "Differential patterns of DNA binding by myc and max proteins" (1993).

43. M. Allevato, *et al.*, Sequence-specific DNA binding by MYC/MAX to low-affinity non-E-box motifs. *PLoS One* **12** (2017).

44. J. Guo, *et al.*, Sequence specificity incompletely defines the genome-wide occupancy of Myc. *Genome Biol* **15** (2014).

45. M. Már, K. Nitsenko, P. O. Heidarsson, Multifunctional Intrinsically Disordered Regions in Transcription Factors. *Chem. Eur. J.* **29**, e202203369 (2023).

46. A. Farina, F. Faiola, E. Martinez, Reconstitution of an E box-binding Myc:Max complex with recombinant full-length proteins expressed in Escherichia coli. *Protein Expr Purif* **34**, 215–222 (2004).

47. S. Schütz, *et al.*, The Disordered MAX N-terminus Modulates DNA Binding of the Transcription Factor MYC:MAX. *J Mol Biol* **434** (2022).

48. W. Fieber, *et al.*, Structure, function, and dynamics of the dimerization and DNA-binding domain of oncogenic transcription factor v-Myc. *J Mol Biol* **307**, 1395–1410 (2001).

49. K. C. Jung, H. S. Rhee, C. H. Park, C. H. Yang, Determination of the dissociation constants for recombinant c-Myc, Max, and DNA complexes: The inhibitory effect of linoleic acid on the DNA-binding step. *Biochem Biophys Res Commun* **334**, 269–275 (2005).

50. T. E. Speltz, *et al.*, Targeting MYC with modular synthetic transcriptional repressors derived from bHLH DNA-binding domains. *Nat Biotechnol* (2022) https:/doi.org/10.1038/s41587-022-01504-x.

51. C. Andresen, *et al.*, Transient structure and dynamics in the disordered c-Myc transactivation domain affect Bin1 binding. *Nucleic Acids Res* **40**, 6353–6366 (2012).

52. M. Welcker, *et al.*, The Fbw7 tumor suppressor regulates GSK3 phosphorylation-dependent cMyc protein degradation_Welcker_PNAS_2004. *PNAS* **101**, 9085–9090 (2004).

53. T. L. Religa, A. M. Ruschak, R. Rosenzweig, L. E. Kay, Site-directed methyl group labeling as an NMR probe of structure and dynamics in supramolecular protein systems: Applications to the proteasome and to the ClpP protease. *J Am Chem Soc* **133**, 9063–9068 (2011).

54. A. S. Krois, H. Jane Dyson, P. E. Wright, Long-range regulation of p53 DNA binding by its intrinsically disordered N-terminal transactivation domain. *Proc Natl Acad Sci U S A* **115**, E11302–E11310 (2018).

55. S. Lee, M. Miller, J. D. Shuman, P. F. Johnson, CCAAT/enhancer-binding protein β DNA binding is auto-inhibited by multiple elements that also mediate association with p300/CREB-binding protein (CBP). *Journal of Biological Chemistry* **285**, 21399–21410 (2010).

56. F. Wang, *et al.*, Biochemical and Structural Characterization of an Intramolecular Interaction in FOXO3a and Its Binding with p53. *J Mol Biol* **384**, 590–603 (2008).

57. B. Bourgeois, *et al.*, Multiple regulatory intrinsically disordered motifs control FOXO4 transcription factor binding and function. *Cell Rep* **36**, 109446 (2021).

58. F. Lorenzin, *et al.*, Different promoter affinities account for specificity in MYC-dependent gene regulation. *Elife*, 15161 (2016).

59. M. Dyla, M. Kjaergaard, Intrinsically disordered linkers control tethered kinases via effective concentration. *Proc Natl Acad Sci USA* **117**, 21413–21419 (2020).

60. W. Borcherds, *et al.*, Optimal Affinity Enhancement by a Conserved Flexible Linker Controls p53 Mimicry in MdmX. *Biophys J* **112**, 2038–2042 (2017).

61. S. F. Banani, H. O. Lee, A. A. Hyman, M. K. Rosen, Biomolecular condensates: Organizers of cellular biochemistry. *Nat Rev Mol Cell Biol* **18**, 285–298 (2017).

62. Y. Shin, C. P. Brangwynne, Liquid phase condensation in cell physiology and disease. *Science (1979)* **357** (2017).

63. A. Boija, *et al.*, Transcription Factors Activate Genes through the Phase-Separation Capacity of Their Activation Domains. *Cell* **175**, 1842-1855.e16 (2018).

64. D. Solvie, *et al.*, MYC multimers shield stalled replication forks from RNA polymerase. *Nature* **612**, 148–155 (2022).

65. Y. Lu, *et al.*, Phase separation of TAZ compartmentalizes the transcription machinery to promote gene expression. *Nat Cell Biol* **22**, 453–464 (2020).

66. N. Schneider, *et al.*, Liquid-liquid phase separation of light-inducible transcription factors increases transcription activation in mammalian cells and mice. *Sci. Adv* **7**, eabd3568. (2021).

67. J. Yang, *et al.*, Phase separation of Myc differentially regulates gene transcription. *bioRxiv* (2022) https:/doi.org/10.1101/2022.06.28.498043.

68. C. Engler, R. Kandzia, S. Marillonnet, A one pot, one step, precision cloning method with high throughput capability. *PLoS One* **3** (2008).

69. K. Pervushin, R. Riek, G. Wider, K. Wüthrich, Attenuated T2 relaxation by mutual cancellation of dipole-dipole coupling and chemical shift anisotropy indicates an avenue to NMR structures of very large biological macromolecules in solution. *Proc Natl Acad Sci* **94**, 12366–12371 (1997).

70. M. Sattler, J. Schleucher, C. Griesinger, Heteronuclear multidimensional NMR experiments for the structure determination of proteins in solution employing pulsed field gradients. *Prog Nucl Magn Reson Spectrosc* **34**, 93–158 (1999).

71. Y. Shen, A. Bax, Prediction of Xaa-Pro peptide bond conformation from sequence and chemical shifts. *J Biomol NMR* **46**, 199–204 (2010).

72. F. A. A. Mulder, D. Schipper, R. Bott, R. Boelens, Altered Flexibility in the Substrate-binding Site of Related Native and Engineered High-alkaline Bacillus subtilisins. *J Mol Biol* **292**, 111–123 (1999).

73. F. H. Schumann, *et al.*, Combined chemical shift changes and amino acid specific chemical shift mapping of protein-protein interactions. *J Biomol NMR* **39**, 275–289 (2007).

74. M. P. Williamson, Using chemical shift perturbation to characterise ligand binding. *Prog Nucl Magn Reson Spectrosc* **73**, 1–16 (2013).

75. S. P. Skinner, *et al.*, CcpNmr AnalysisAssign: a flexible platform for integrated NMR analysis. *J Biomol NMR* **66**, 111–124 (2016).

Figures and Tables

Figure 1.

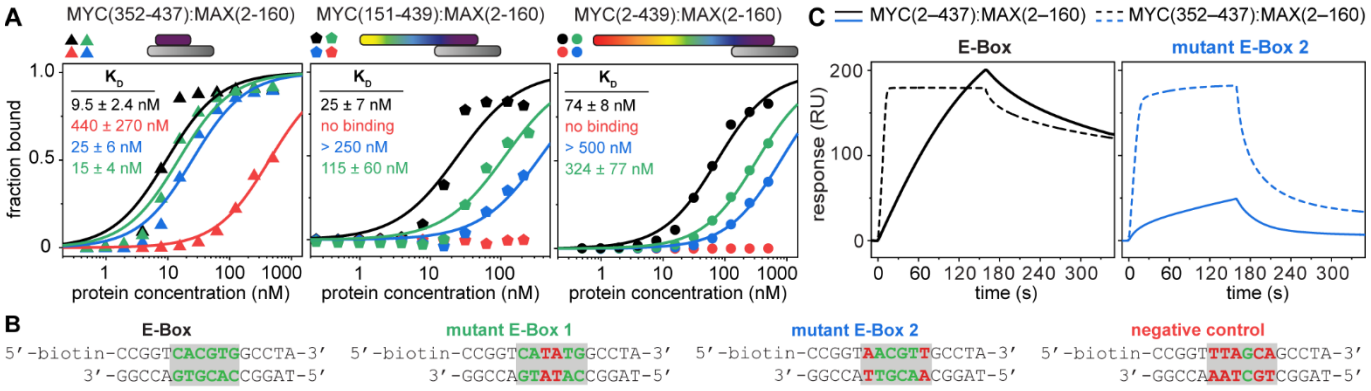

B

E-Box	mutant E-Box 1	mutant E-Box 2	negative control
5′-biotin-CCGGTCACGTGGCCTA-3′	5′-biotin-CCGGTCATATGGCCTA-3′	5′-biotin-CCGGTAACGTTGCCTA-3′	5′-biotin-CCGGTTTAGCAGCCTA-3′
3′-GGCCAGTGCACCGGAT-5′	3′-GGCCAGTATACCGGAT-5′	3′-GGCCATTGCAACGGAT-5′	3′-GGCCAAATCGTCGGAT-5′

Disordered regions in MYC reduce the affinity for DNA and provide specificity for the cognate E-Box sequence. *(A) Steady-state affinity analysis for binding of MYC(352–437):MAX(2–160) (left, triangles), MYC(151–439):MAX(2–160) (middle, pentagons) and MYC(2-439):MAX(2–160) (right, circles) to immobilized E-Box (black), mutant E-Box 1 (green), mutant E-Box 2 (blue) or a negative control DNA (red). Values represent mean K_D ± SD obtained from a fit (solid lines) with equation (3), assuming a 1:1 binding model. Schematics of the MYC:MAX complexes are shown above the graphs, where MAX is in greyscale and MYC is colored with a rainbow gradient. (B) Duplex DNA oligonucleotides used in the SPR experiments. The core E-Box hexamer is in green with gray background, altered nucleotides are in red. (C) Representative SPR sensorgrams for binding of MYC(2-439):MAX(2–160) and MYC(352–437):MAX(2–160) (solid and dotted lines, respeectively) to E-Box (left, black) and mutant E-Box 2 DNA (right, blue) at 62.5 nM protein concentration, illustrating the reduced association rates for the full-length complex.*

Figure 2.

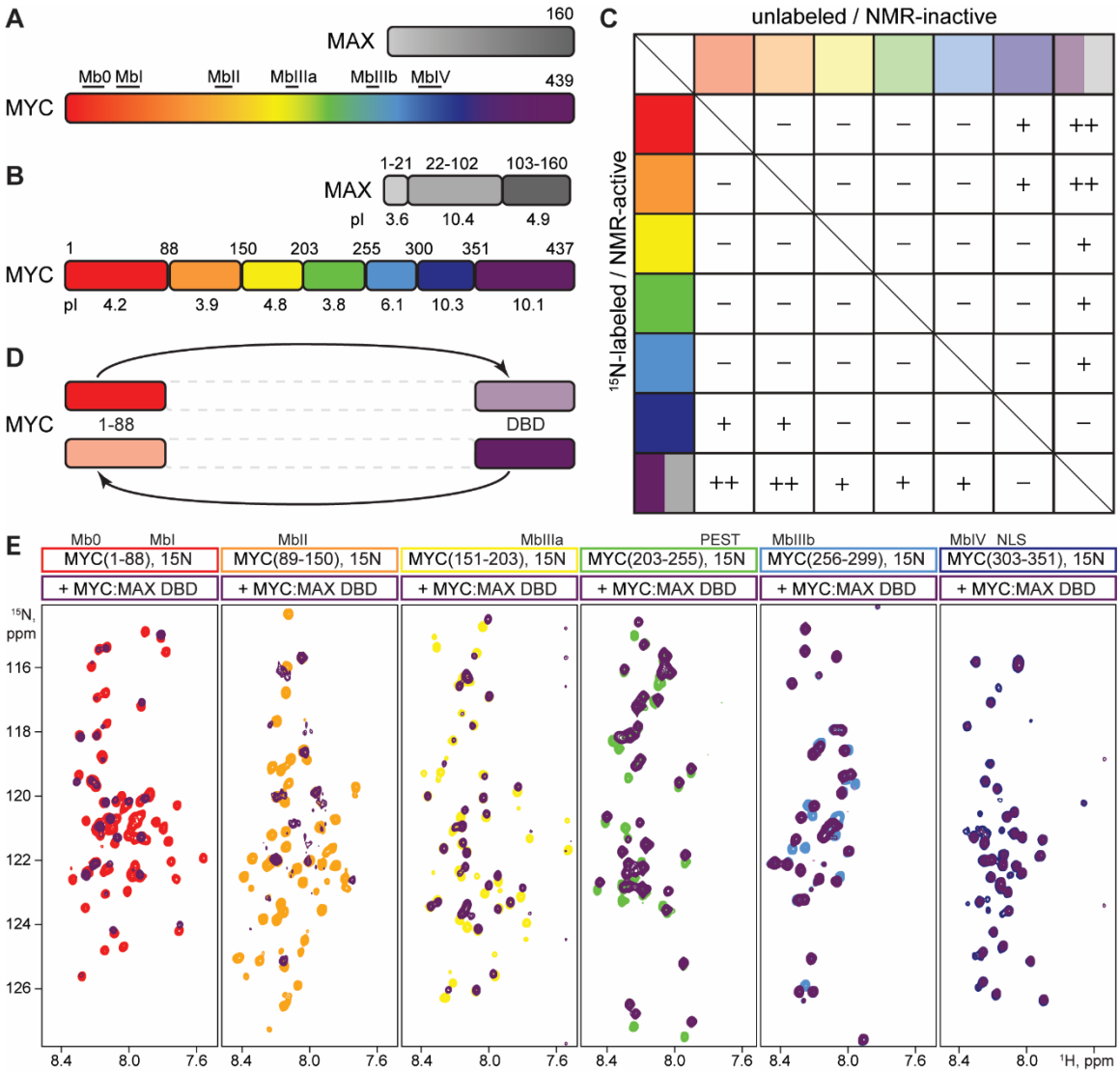

Disordered and structured regions of MYC interact with each other: *(A) Schematic representation of full-length MYC and MAX. Locations of the conserved MYC Box (Mb) motifs are indicated. (B) Fragmentation of MYC to obtain well-expressing, soluble proteins. MYC(352–437) (purple) contains the bHLH-LZ motif, which heterodimerizes with the respective motif in MAX(22–102) (grey), thereby forming the DNA binding domain. The isoelectric points and fragment boundaries are indicated. (C) Summary of NMR binding experiments and MYC:MYC interactions identified in this study. ^{15}N-labeled MYC fragments (bright colors) were tested for binding to all other (unlabeled) fragments (pale colors). "+" denotes binding (presence of CSPs), "++" denotes strong binding (CSPs observed and significant decrease in signal intensities) and "–" denotes no binding (absence of CSPs at 500 µM ligand concentration). The bipartite purple and grey field denotes the heterodimeric MYC(352–437):MAX(22–102) complex (henceforth MYC:MAX DBD). (D) NMR binding results are consistent regardless of which fragment is NMR-active. (E) ^{1}H-^{15}N HSQC spectra of 50 µM ^{15}N-labeled MYC fragments in absence (red: MYC(1–88), orange: MYC(89–150), yellow: MYC(151–203), green: MYC(203–255), blue: MYC(256–299), dark blue: MYC(303–351)) and in presence of a 10-fold molar excess of the MYC:MAX DBD (purple). Presence of CSPs or decrease in peak intensities indicates binding. This dataset corresponds to the last column of the matrix shown in (C).*

. **Figure 3.**

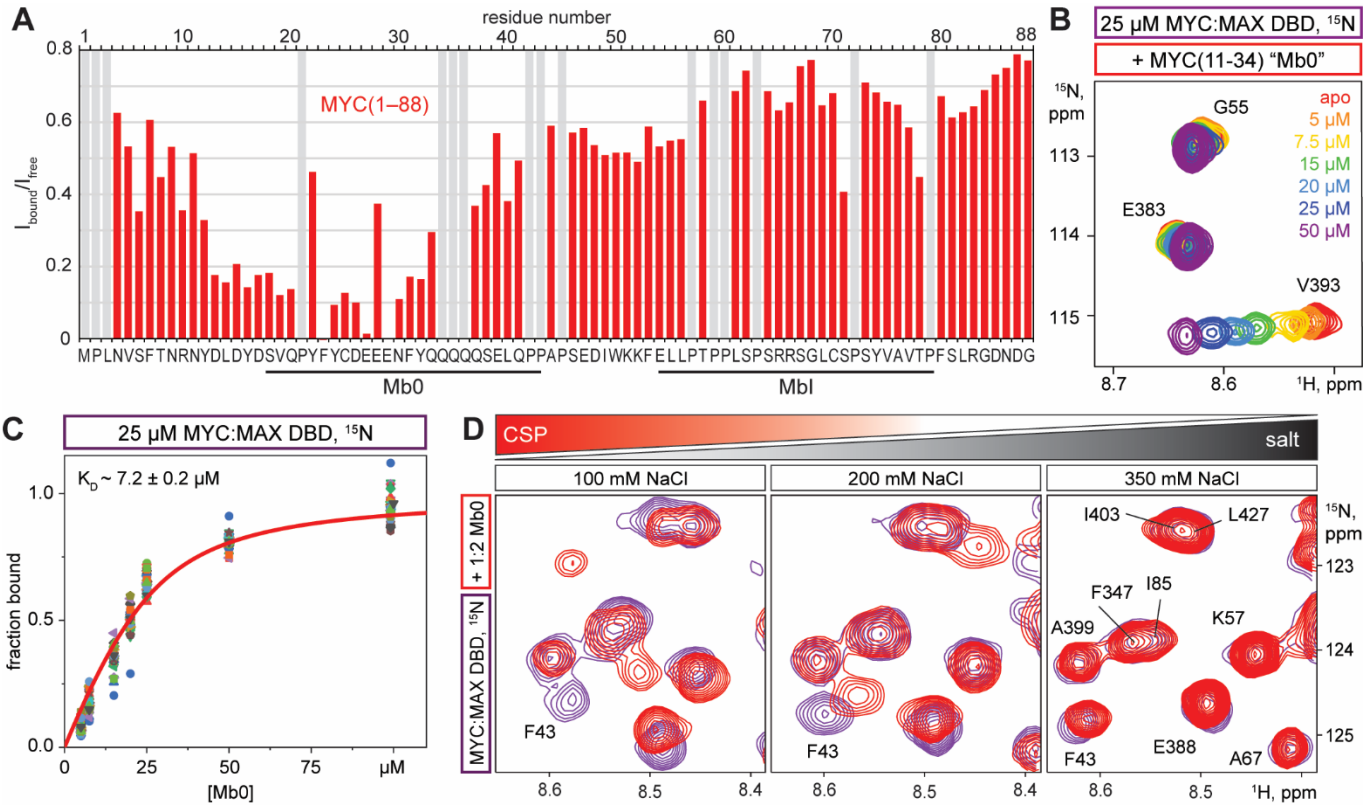

Characterization of the interaction between Mb0 and the MYC:MAX DBD. *(A) Binding of MYC:MAX DBD to ^{15}N-labeled MYC(1–88). Plots of I_{bound}/I_{free} intensity ratios against the amino acid sequence reveal binding sites when the ratios deviate substantially from 1, as observed for residues in the conserved Mb0 motif. The MbI is not affected. (B) Zoom on ^{1}H-^{15}N TROSY spectra of 25 μM MYC:MAX DBD in presence of increasing concentrations of unlabeled Mb0 peptide indicated by gradual coloring from red (0 μM) to purple (50 μM). Full spectra are shown in SI Appendix, Fig. S9A. (C) Analysis of NMR titration data for the interaction shown in (B). The K_D ± SD is obtained from fitting the titration data globally (red line) with equation (2). (D) Zoom on ^{1}H-^{15}N TROSY spectra of 25 μM ^{15}N-labeled MYC:MAX DBD in absence (purple) and presence of 50 μM Mb0 peptide (red) in buffer containing 100, 200 or 350 mM NaCl (from left to right).*

Figure 4.

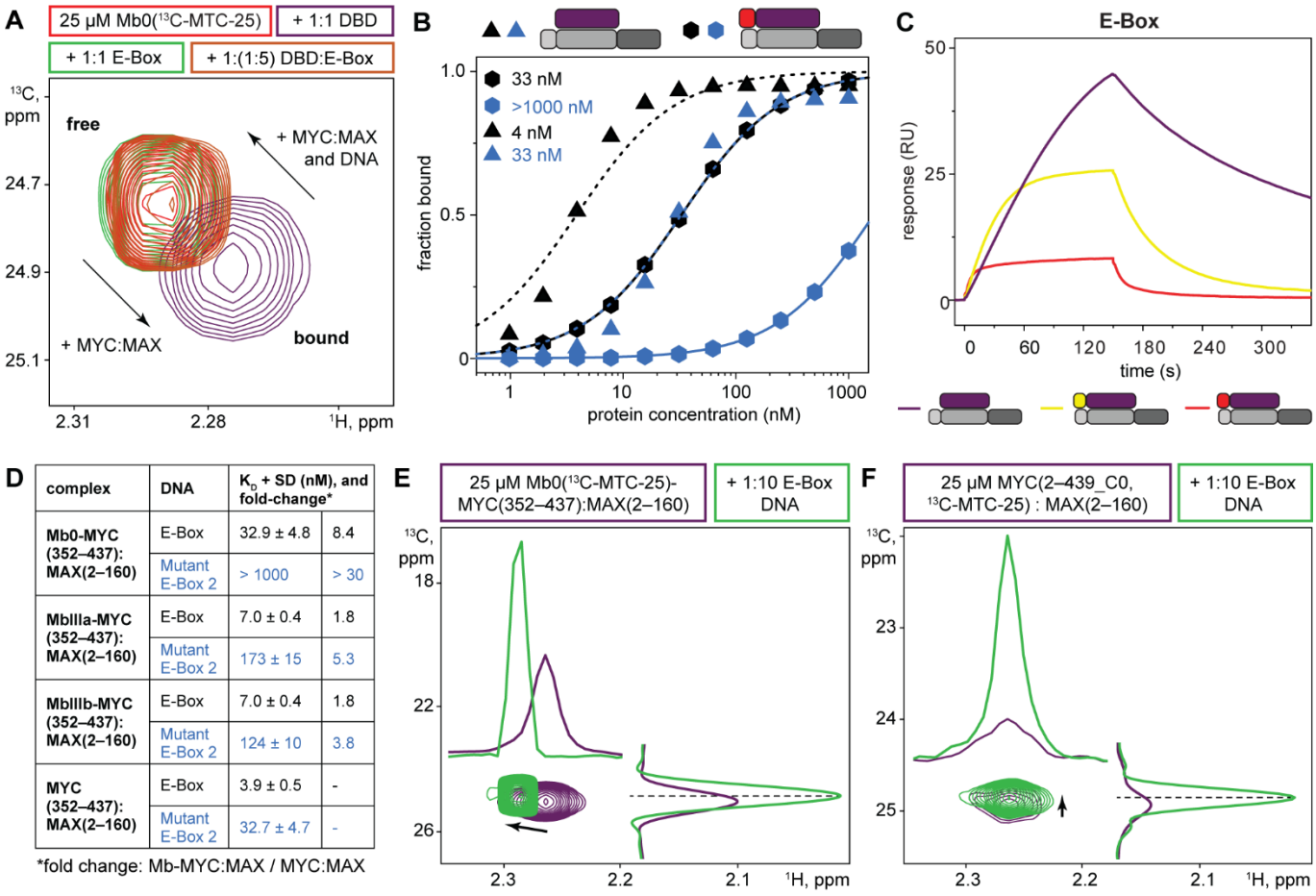

Figure 1. MYC boxes and E-Box DNA compete for a mutual binding site on the MYC:MAX DBD. (A) *^{1}H-^{13}C HMQC spectra of 25 µM Mb0, that is ^{13}C-Methylthiocystein (MTC)-labeled at residue 25, in its free form (red) or in presence of equimolar amounts of E-Box DNA (green) and MYC:MAX DBD (purple) or in a 1:1:5 ratio (brown) with DBD and E-Box-DNA. (B) Steady-state analysis for the binding of MYC(352–437):MAX(2–160) (triangles, dotted lines) and Mb0-MYC(352–437):MAX(2–160) (hexagons, solid lines) to immobilized E-Box (black) and mutant E-Box 2 DNA (blue). K_D ± SD values are obtained from a global fit with equation (3), assuming a 1:1 binding model. (C) Representative SPR sensorgrams for binding of MYC(352–437):MAX(2–160) (purple), as well as of Mb0- (red) or MbIIIa- (yellow) fusions thereof, to E-Box DNA at 3.9 nM protein concentration, illustrating the accelerating effect of the directly tethered MYC boxes on the dissociation rate. (D) Summary of K_D values ± SD from equilibriums fits in (B) and SI Appendix, Fig. S14B. Fold-change values are with respect to MYC(352–437):MAX(2–160). (E, F) ^{1}H-^{13}C HMQC spectra of (E) 25 µM Mb0-MYC(352–437):MAX(2–160) and (F) 25 µM full-length MYC:MAX that are ^{13}C- MTC-labeled at MYC residue 25 in absence (purple) and presence (green) of a 10-fold molar excess of E-Box DNA. 1D cross-sections in the ^{1}H and ^{13}C dimension are shown to illustrate the increase in peak intensity upon addition of DNA.*

Figure 5.

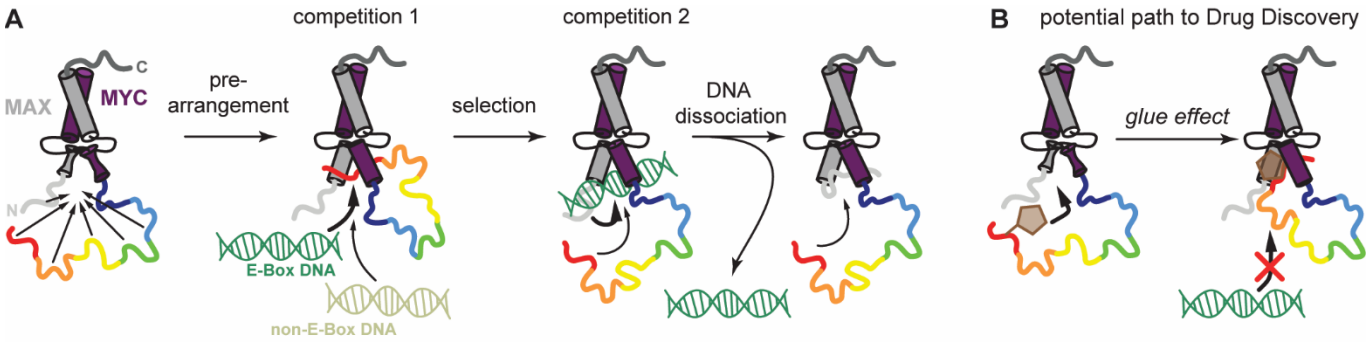

Figure 2: Intramolecular interactions in MYC provide DNA selectivity and offer new paths to drug discovery. *(A) Schematic depiction of our current model how DBD-interacting Mb motifs influence the DNA binding behavior of MYC:MAX. See Discussion for a more detailed explanation. (B) Potential new approach to directly target MYC:MAX by exploiting the interactions identified in this work with covalent drug modalities that stabilize the MYC box : DBD interactions, resulting in further reduced DNA binding.*

***Table 1**. Summary of NMR-derived K_D values for MYC:MYC interactions described in this study.*

NMR-active	**NMR-inactive**	**K_D ± SD**
MYC:MAX DBD	MYC(11–34) = Mb0	7.2 ± 0.2 μM
MYC:MAX DBD	MYC(203–255), contains PEST	49 ± 1 μM
MYC(256–299), contains MbIIIb	MYC:MAX DBD	361 ± 13 μM
MYC(151–203), contains MbIIIa	MYC:MAX DBD	518 ± 16 μM
MYC(303–351), contains MbIV	MYC(1–88), contains Mb0+MbI	> 1000 μM (1205 ± 62 μM)